Figure 4-2

GALAXY MobileStar Digital
Modulator Block Diagram
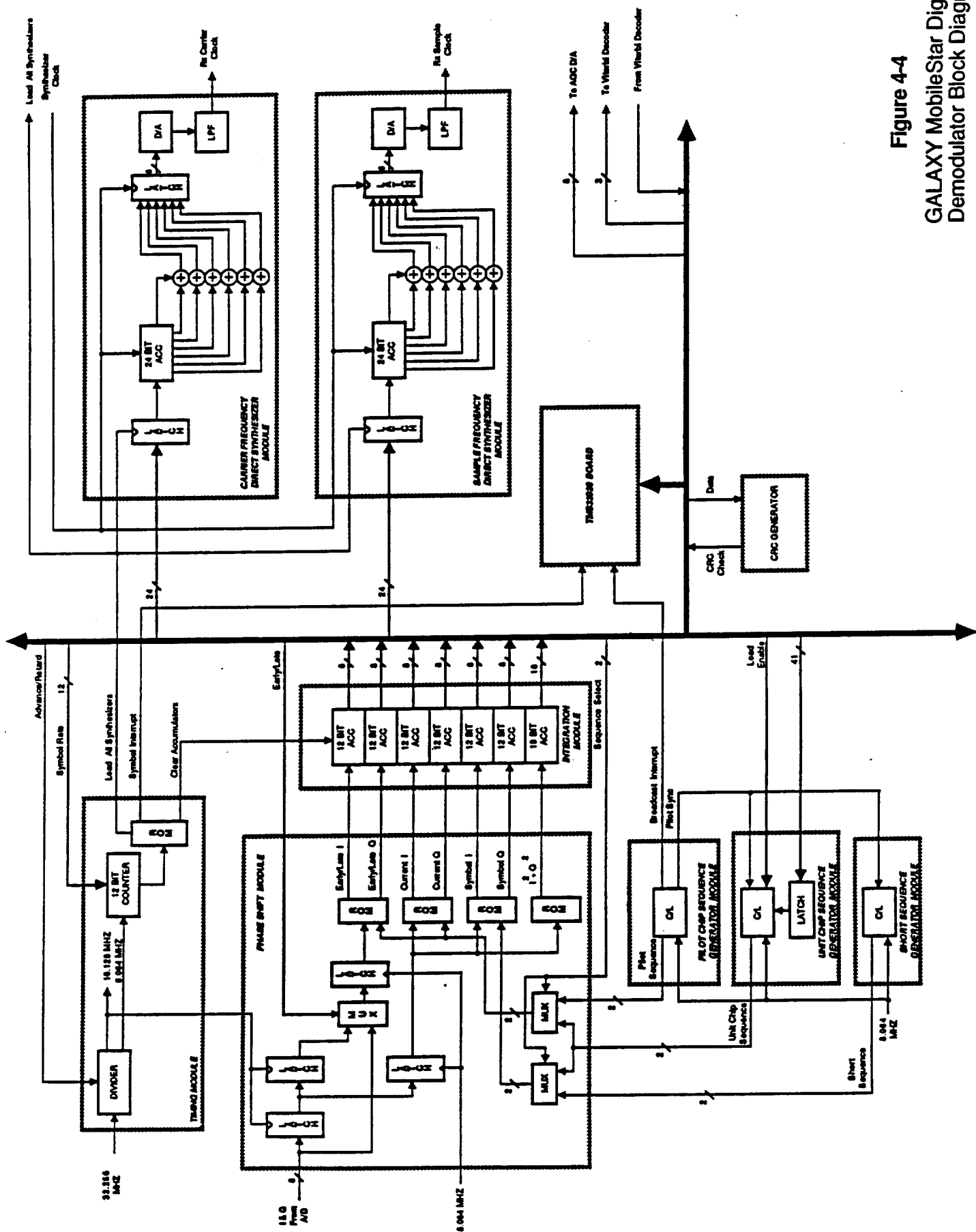
Figure 4-3

GALAXY MobileStar Demodulator Block Diagram

Figure 4-4
GALAXY MobileStar Digital
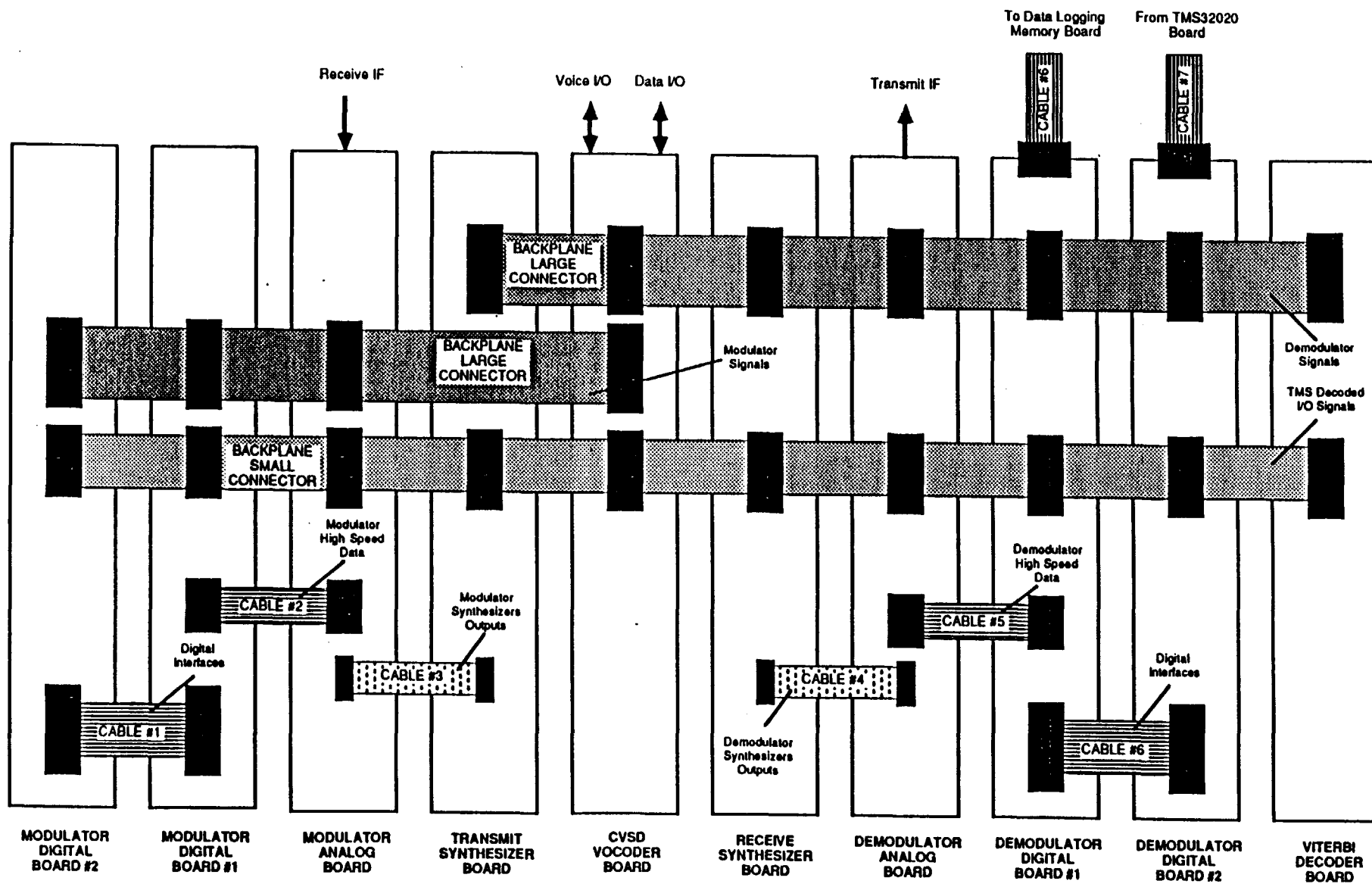Demodulator Block Diagram

Figure 4-5

GALAXY MobileStar Demonstration Modem Board Interconnections

Hub to Mobile Implementation and Simulation

The Hub to Mobile processes modeled by the simulation are shown in Fig.5-1. In Fig.5-2 the actual simulation flow is shown, the two block diagrams are mathematically equivalent when the noise variables are properly defined. For instance, in Fig.5-1 three independent noise sources termed "Other Users" and three independent Thermal Noise sources are shown. The independence of all six noise sources follows from the fact that the Thermal noise and "Other Users" noise are clearly independent and from the fact that the three signal flow paths shown in the figure are processed by different PN sequences, which makes the different random processes independent with good approximation. For instance, the upper path, representing the data path, is processed by the long 41-bit PN sequence, whereas the middle path is processed by the pilot 4095 PN sequence, and the last path leading to the AGC tracking loop is not processed by a PN sequence altogether.

In Fig.5-2 the six noise sources have been reduced to three but the variance of the noise has been adjusted to take into consideration the fact that, in the Hub to Mobile link, when the signal fades so does the "Other Users" noise, whereas the thermal noise at the front end of the receiver does not. Given the ratio between "Other Users" noise power and thermal noise power, i.e. I_o/N_o, the variance of the noise samples is adjusted according to the following formula

$$\text{Variance} = \frac{N_o + G_f^2 I_o}{2}$$

where G_f is the magnitude of the fading variables. It is clear that the carrier phase complex multiply can be interchanged in position with the additive noise without altering the statistical properties of the noise.

Following the additive noise and gain adjustment, the signals are quantized and fed to three tracking loops, which will be described in the following, and to the deinterleaver and Viterbi decoder. Prior to the Viterbi decoding of the data, a preamble detector determines if data is present or not present in the incoming frame. Also, a transition from 1 to 0 in the preamble indicates that the incoming frame does not contain data and that the tail symbols will be processed by the decoder. Since phase coherence can be maintained at all times in the hub to mobile link, due to the presence of the pilot, the preamble is not DPSK modulated, as was the case for the mobile to hub link, but simply BPSK modulated. Furthermore, because of the better performance of coherent demodulation the preamble length is only twenty symbols, i.e. the P1 portion shown in Fig.6-1 is not used in the hub to mobile link.

Mobile Phase Tracking Loop

The phase tracking loop is a second order loop with damping factor equal to $1/\sqrt{2}$ for optimal acquisition performance, a block diagram of the loop is given in Fig.5-3. In Fig.5-4 the frequency acquisition performance is shown for two different loop bandwidths and -20 dB and -23 dB of pilot SNR. The phase detector uses the pilot in-quadrature component Q to generate an error signal for the loop. The 8-bit Q samples are then filtered (TMS32020) and a final 24-bit correction sample is provided to the digital frequency synthesizer at the symbol rate.

The loop bandwidth will be set at 1572 Hz. In absence of fading this choice ensures that the phase jitter will be less than 9°, a loss less than 0.1 dB for BPSK. In a fading environment, since the loop bandwidth is roughly 10 times the fading bandwidth (at a vehicle speed of 15 m/s), the loop will be able to track the faded signal in phase. This provides a substantial improvement with respect to a slower loop which is unable to track the phase of the faded signal.

Mobile Timing Tracking Loop

The system timing is derived from a second order tau-dither tracking loop, a block diagram of the loop is shown in Fig.5-5. The hardware provides the TMS32020 with two 8-bit numbers at half the symbol rate. The two values represent the output of the matched filter at the sampling time minus $T_c/2$ (early sample) and plus $T_c/2$ (late sample), where T_c is the chip time. The system impulse response (at the output of the matched filter) is shown in Fig.5-6. The timing error is generated from the early and late samples by taking the difference of the squares of the I and Q early and late samples, i.e. the error is equal to $I^2(E) + Q^2(E) - I^2(L) - Q^2(L)$. By first squaring the samples any carrier phase dependence on the timing error is removed. The phase detector characteristic is shown in Fig.5-6.

The timing loop, as was the case for the phase loop, is designed to have a damping value equal to $1/\sqrt{2}$. Two sets of loop filter gains are used one for acquisition and one for tracking. The loop bandwidth during acquisition is equal to 100 Hz and to 25 Hz during tracking.

Mobile AGC Loop

Proper signal level at the input of the A/D converters is provided by a first order AGC loop.

This loop can be viewed as a noise only gain control since the SNR is about -26 dB at 9600 bps. The noise energy is measured by summing the squares of the in-phase and quadrature components over one symbol period. The resulting samples are filtered and a final correction value is applied to the variable gain amplifier which drives the input signal within the range of the ADC's. In particular, the parameters of the AGC are such that 5 times the standard deviation of the random process at the input of the ADC equals the range of the ADC and the total dynamic range is equal to 25.5 dB.

The loop bandwidth is set to 1100 Hz thus providing adequate gain tracking of the faded signal while maintaining the gain jitter within 0.3 dB.

Fading Model

The random variables used by the simulation program to model the fading processes are generated as follows. The I and Q components of the Rayleigh Fading Generator shown in Fig.2-3 are Gaussian random variables obtained by sampling a Gaussian random process, with a 6-th order Butterworth spectrum and cutoff frequency $F_c = 10$ cycles/meter, at a sampling rate $F_s = 50$ cycles/meter. With a vehicle speed equal to 15 meter/sec. this corresponds to a process with a bandwidth of 150 Hz. In order to generate the I and Q samples at the symbol rate, a 2-nd order Butterworth interpolating filter is used.

The interpolating filter is designed to have a cutoff bandwidth $F_c = 14$ cycles/meter, which is sufficient to practically eliminate the images, at multiples of $F_s=50$ cycles/meter, generated by the original filter. Fig.5-7 shows the frequency response of the original filter, with one image at $F_s=50$ superimposed to the frequency response of the interpolating filter.

Similarly, a third Gaussian process, with a 6-th order Butterworth spectrum and cutoff frequency $F_c=5$ cycles/meter, is generated and again interpolated by the same filter previously discussed. The resulting random variables are then transformed according to a LogNormal distribution with given mean and standard deviation and finally used to model the effects of shadowing on the specular component of the signal.

Hub to Mobile Link: Simulation Results

In Figs.5-8 - 5-10 the simulation results are presented. In Fig.5-8 five bit error rate curves are plotted. This figure shows the insignificant degradation (0.03 dB at an error rate equal to 10^{-3}) of the rate $R_c=12/35$ punctured code with respect to the original $R_c=1/3$ code. Both these curves were generated by modeling the channel as an AWGN channel with perfect synchronization both in phase and time and optimal AGC setting. The third curves shows the degradation due to modem implementation, i.e. phase and time jitter, quantization effects, and gain jitter.

Finally, the last two curves show the effect of Ricean fading and shadowing on the error performance of the system. The set of data for both these curves were generated assuming a ratio of specular to diffuse power equal to 10 dB, i.e. $K_f=10$. In one case the effect of shadowing was not present, whereas the last curve shows the degradation due to shadowing when the LogNormal distribution has a mean attenuation equal to 0 dB and a standard deviation equal to 3 dB.

Fig.5-9 shows the same results just discussed, together with a new curve. This curve shows the effect of severe shadowing on the bit error rate, in this case the LogNormal distribution has a mean attenuation equal to 7.5 dB.

Finally, Fig.5-10 is equivalent to Fig.5-9, in that the same system parameters were used, except that now the frame error rate rather than the bit error rate is plotted.
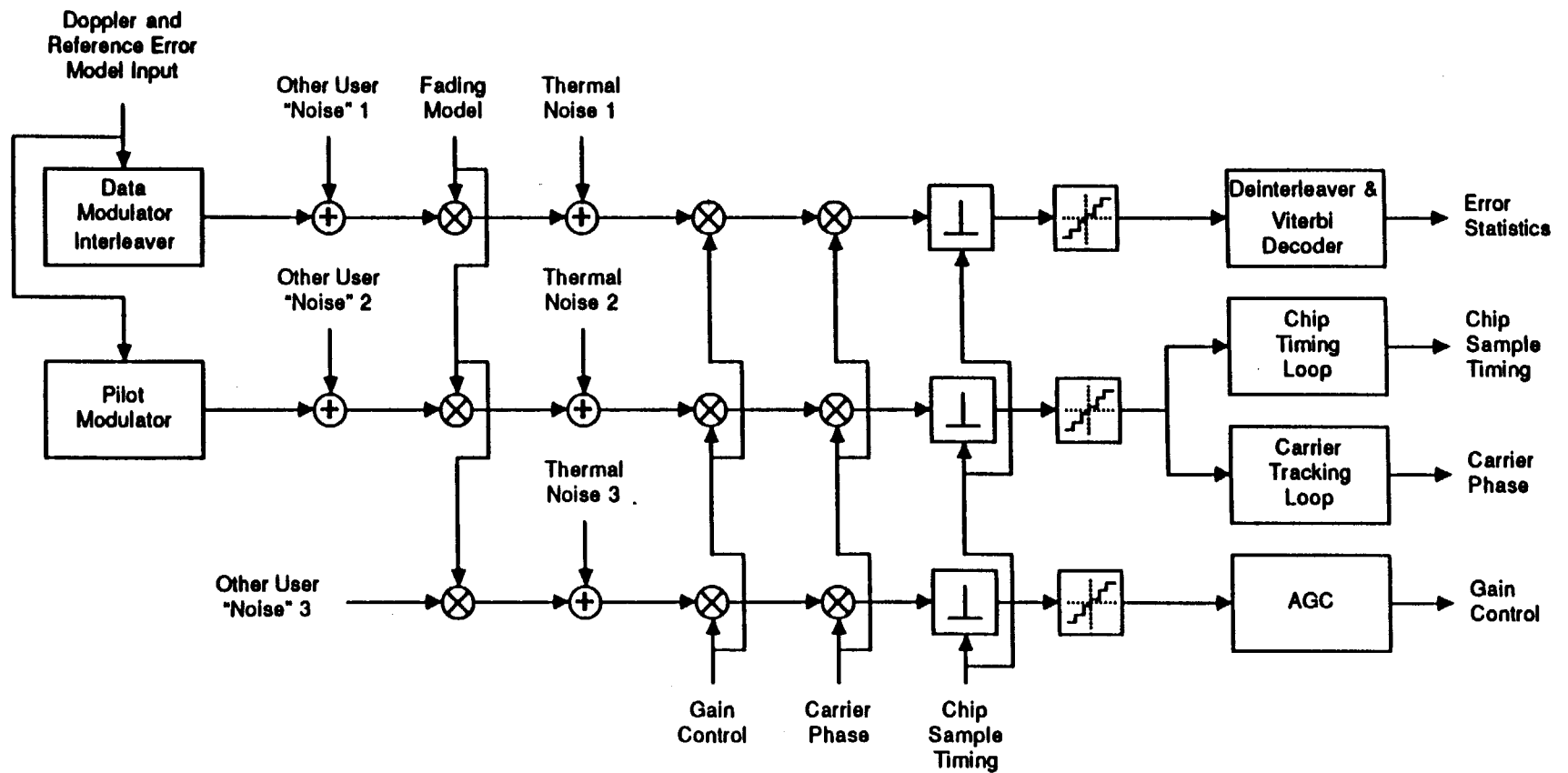
Figure 5-1

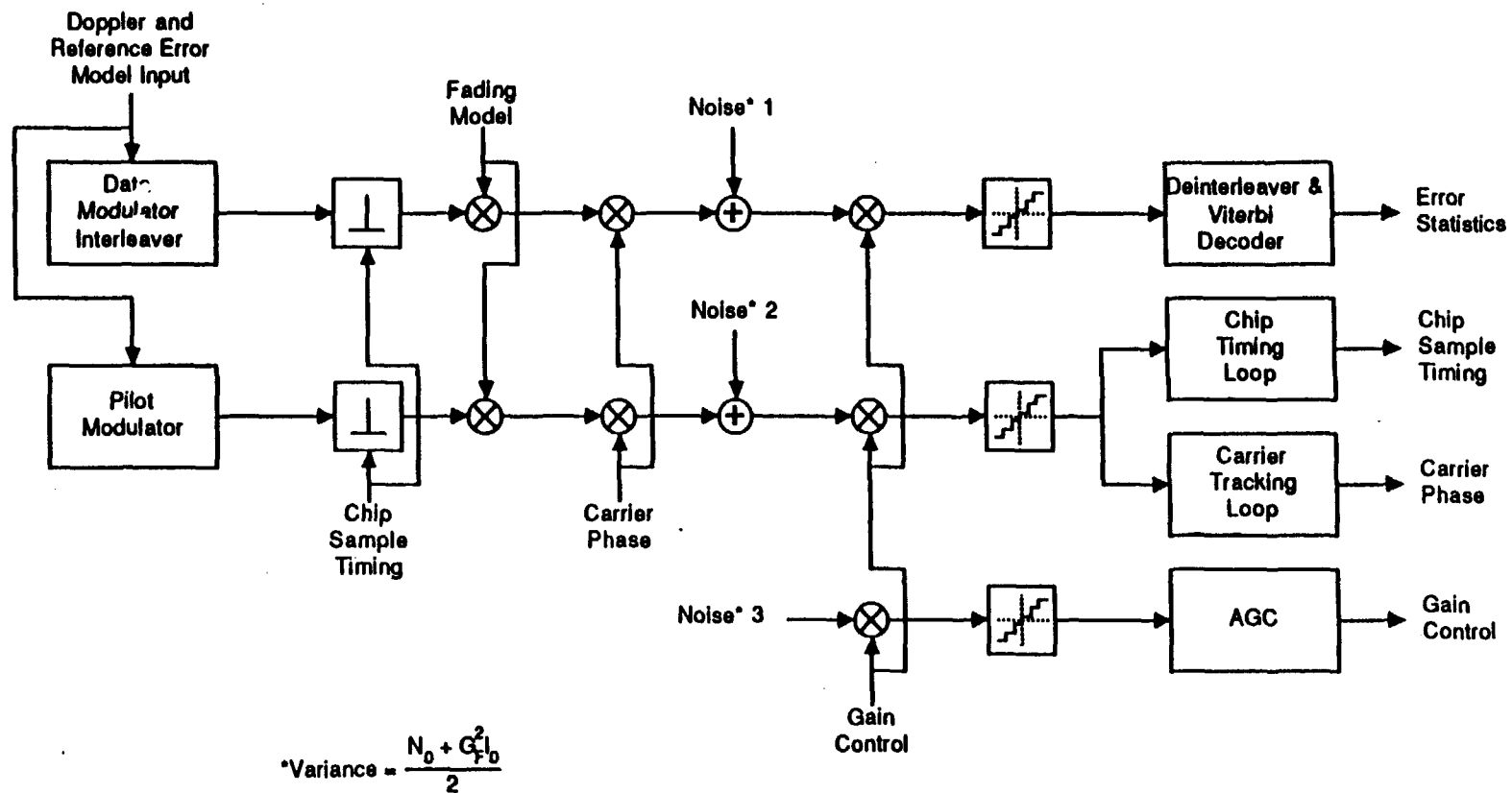Hub to Mobile Processes Modeled by Simulation
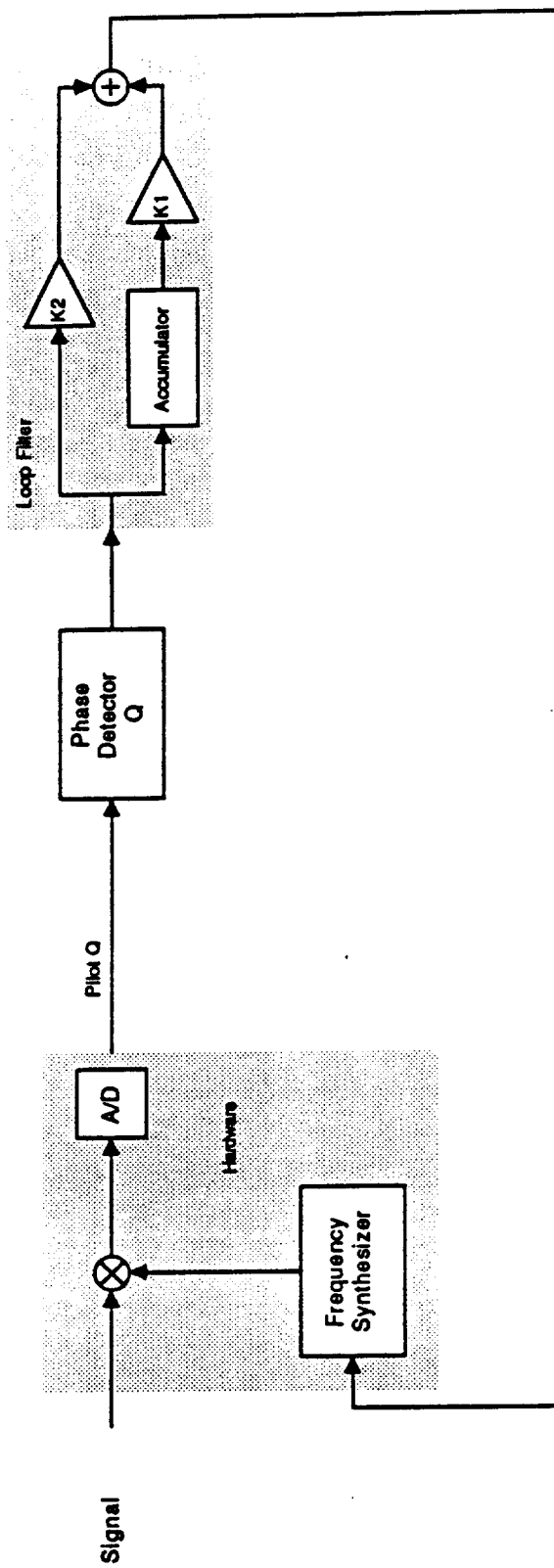
Figure 5-2

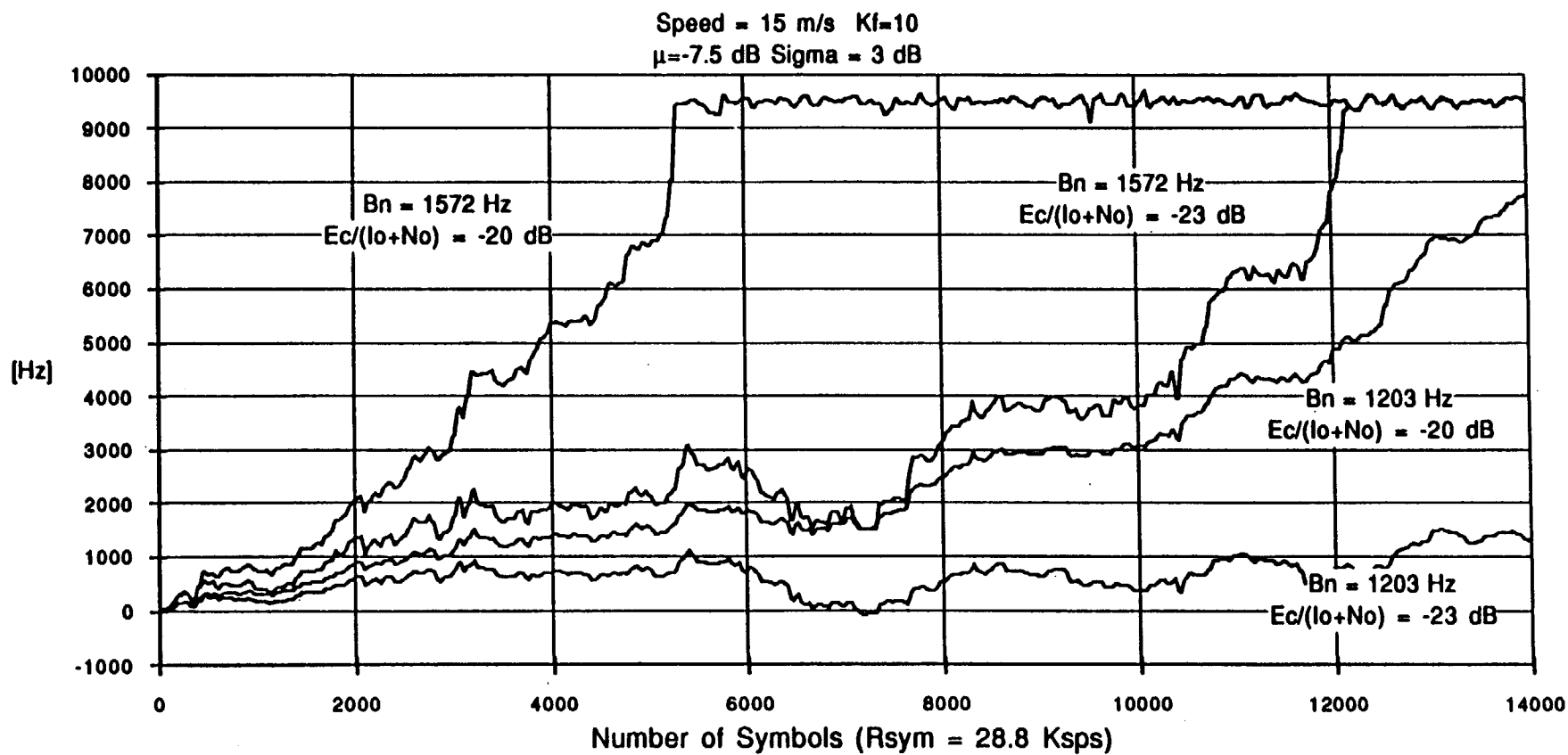**Hub to Mobile Simulation Flow**

Figure 5-3
Mobile Phase Lock Loop

Figure 5-4
Frequency Acquisition

PILOT Signal

A/D

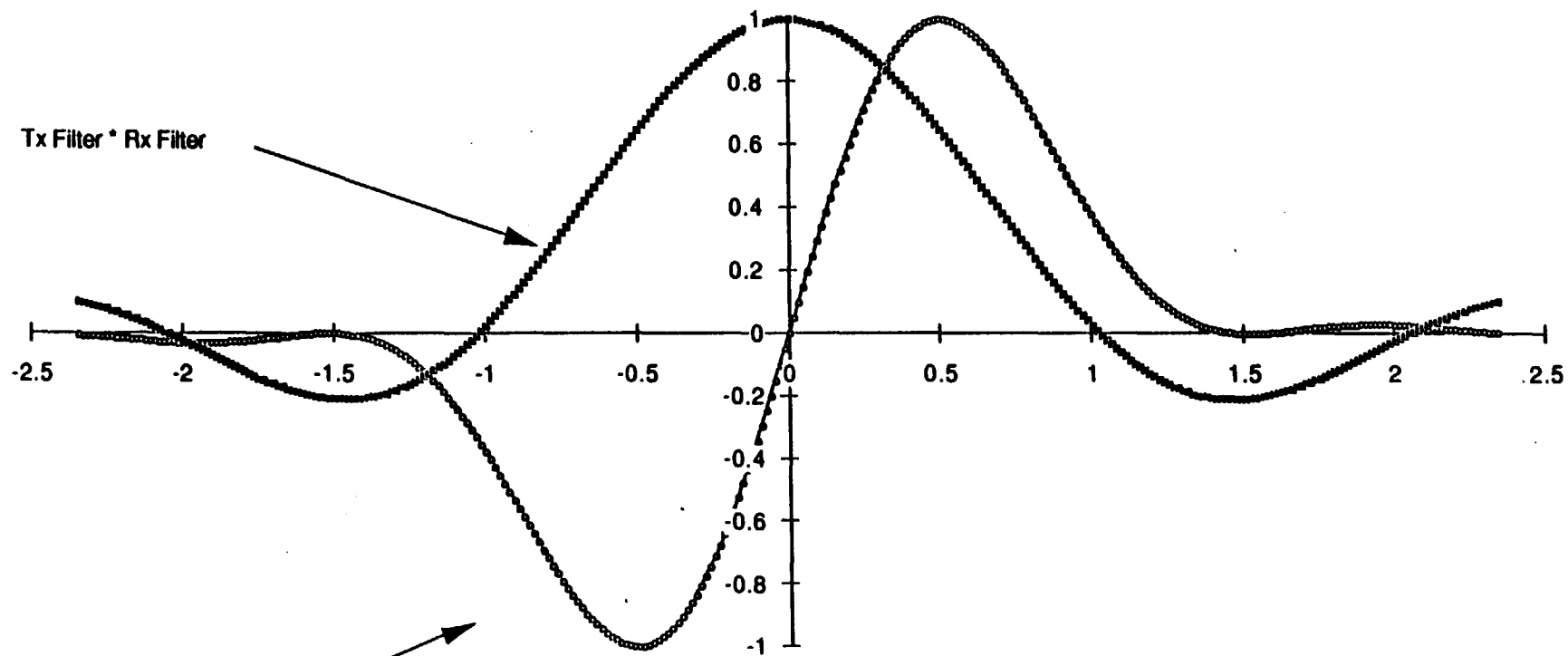Early Late Mux

EARLY I*I + Q*Q

LATE I*I + Q*Q

Loop Filter

K2

K1

Accumulator

Kvco

Frequency Synthesizer

Hardware

Note: The section outlined as hardware was simulated in the modem simulation program. It will be hardware in the demonstration modem.

Figure 5-5
Mobile Time Tracking Loop

Tx Filter * Rx Filter
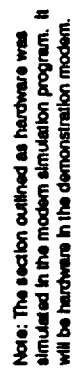
Time Detector Characteristic

Figure 5-6

System Impulse Response and Time Detector
Characteristic
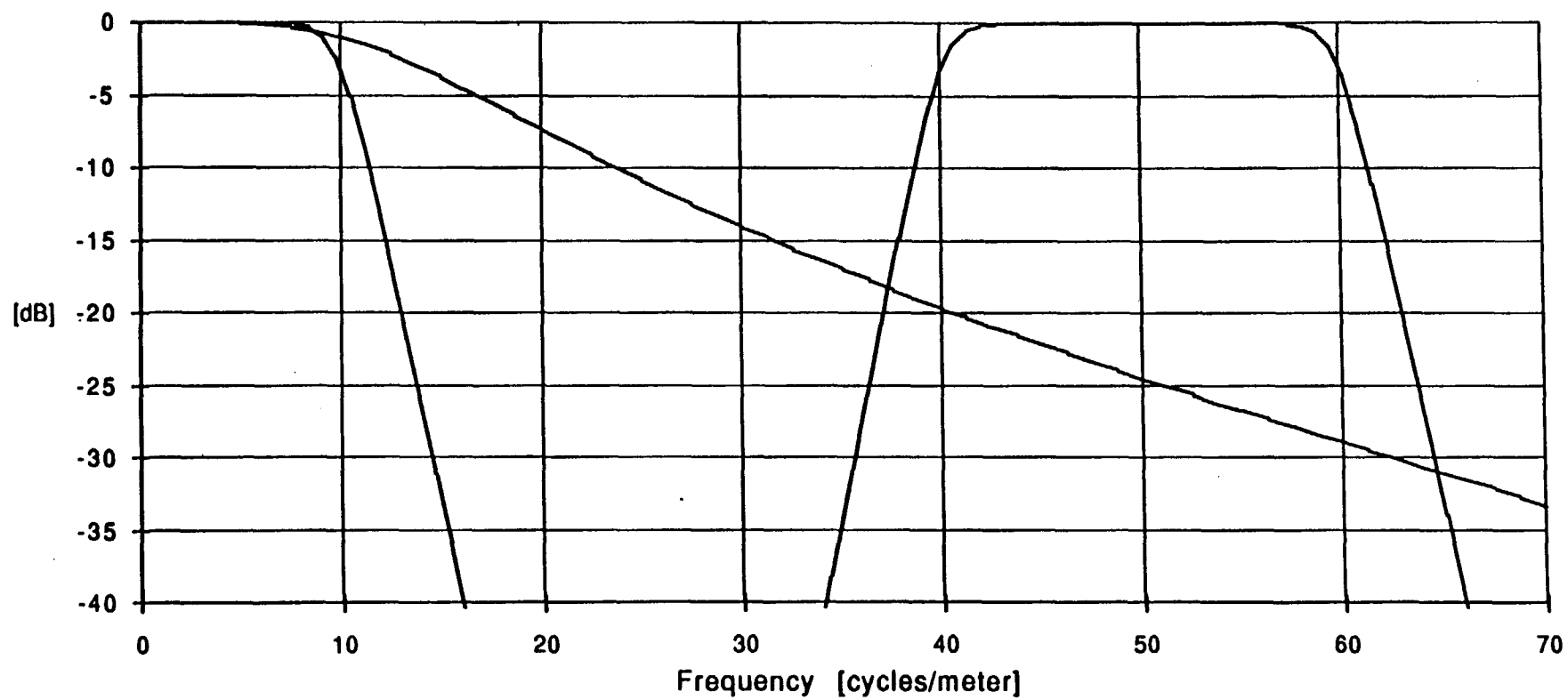
Figure 5-7
Fading and Interpolating Filters
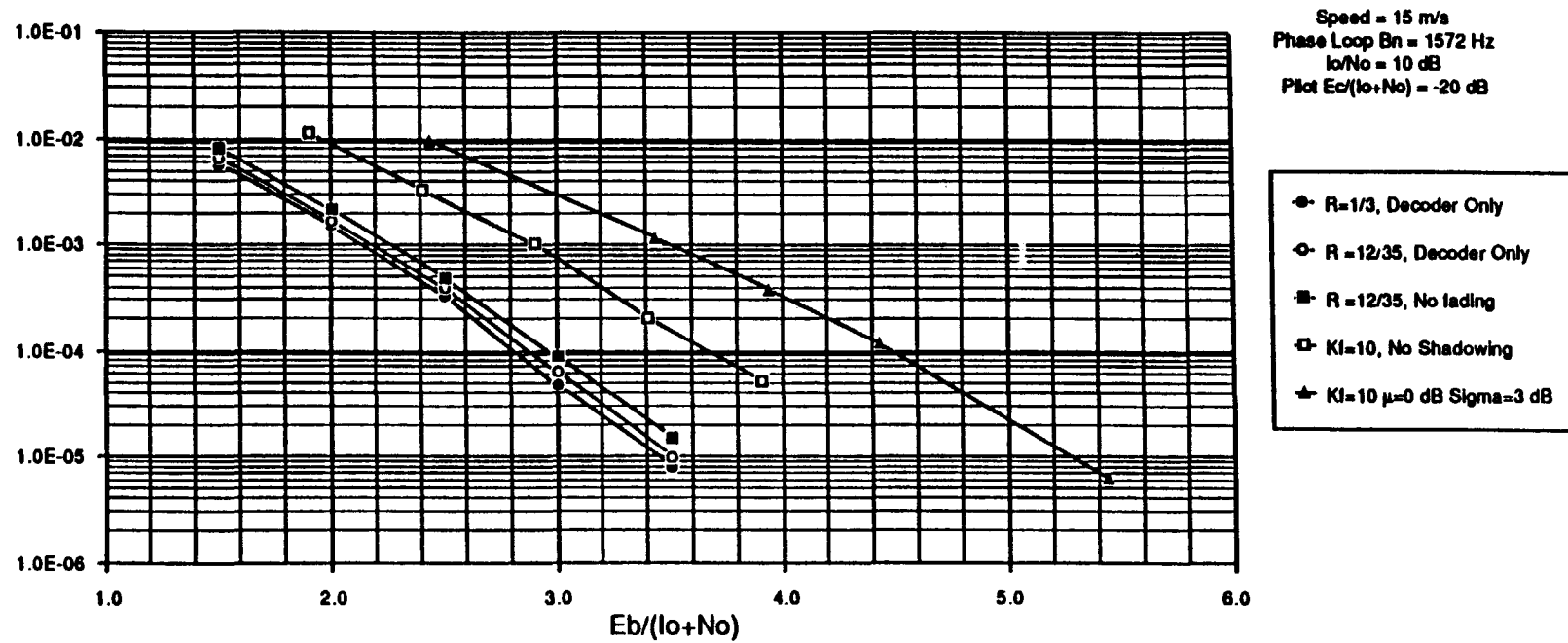
Figure 5-8
Hub to Mobile Link: Bit Error Rate
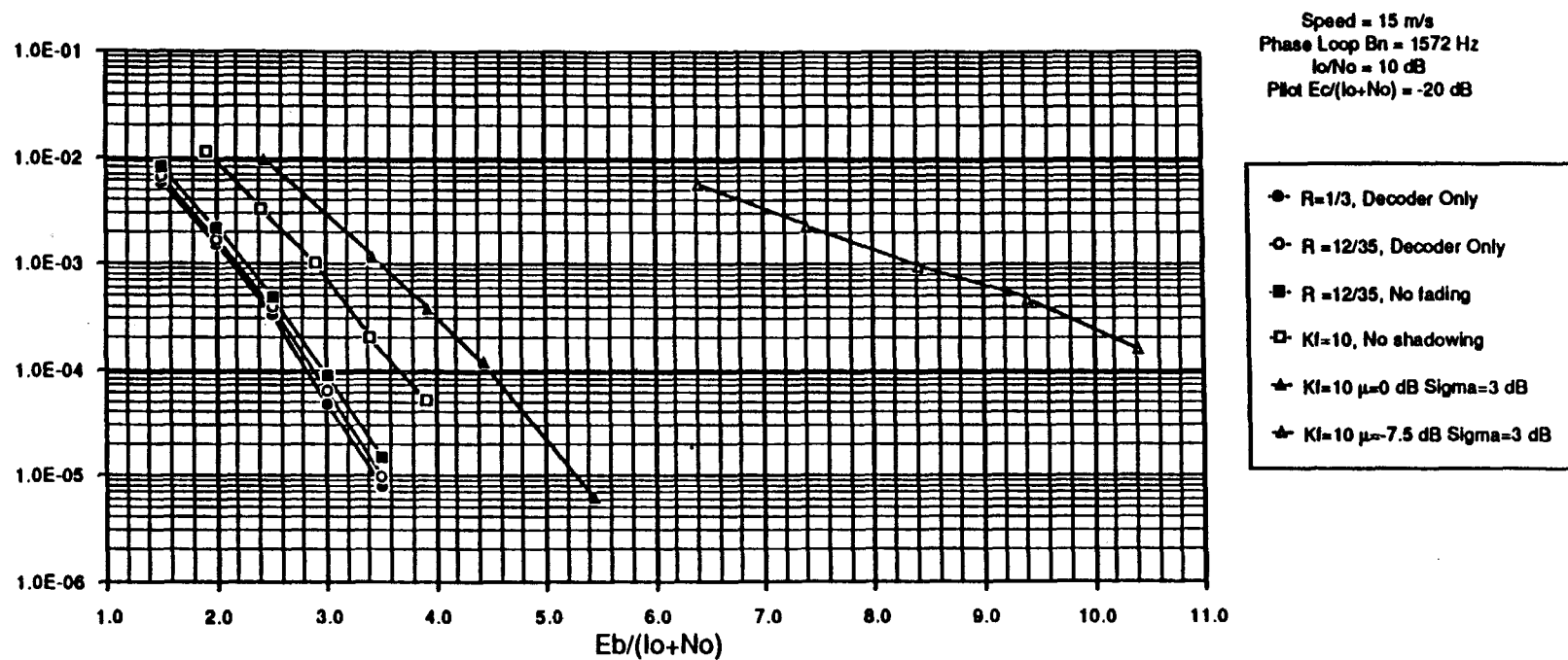
Figure 5-9
Hub to Mobile Link: Bit Error Rate
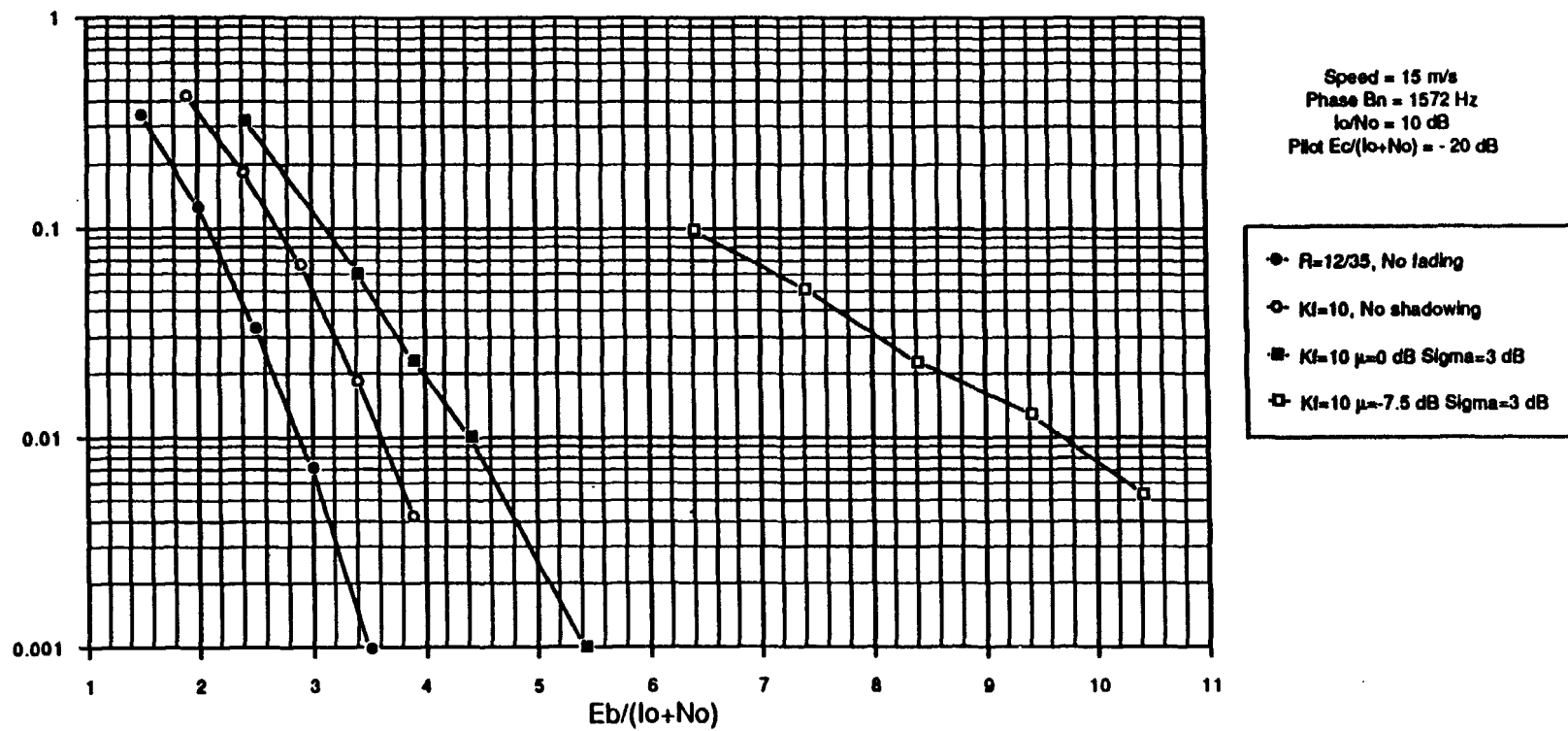
Figure 5-10
Hub to Mobile Link: Frame Error Rate
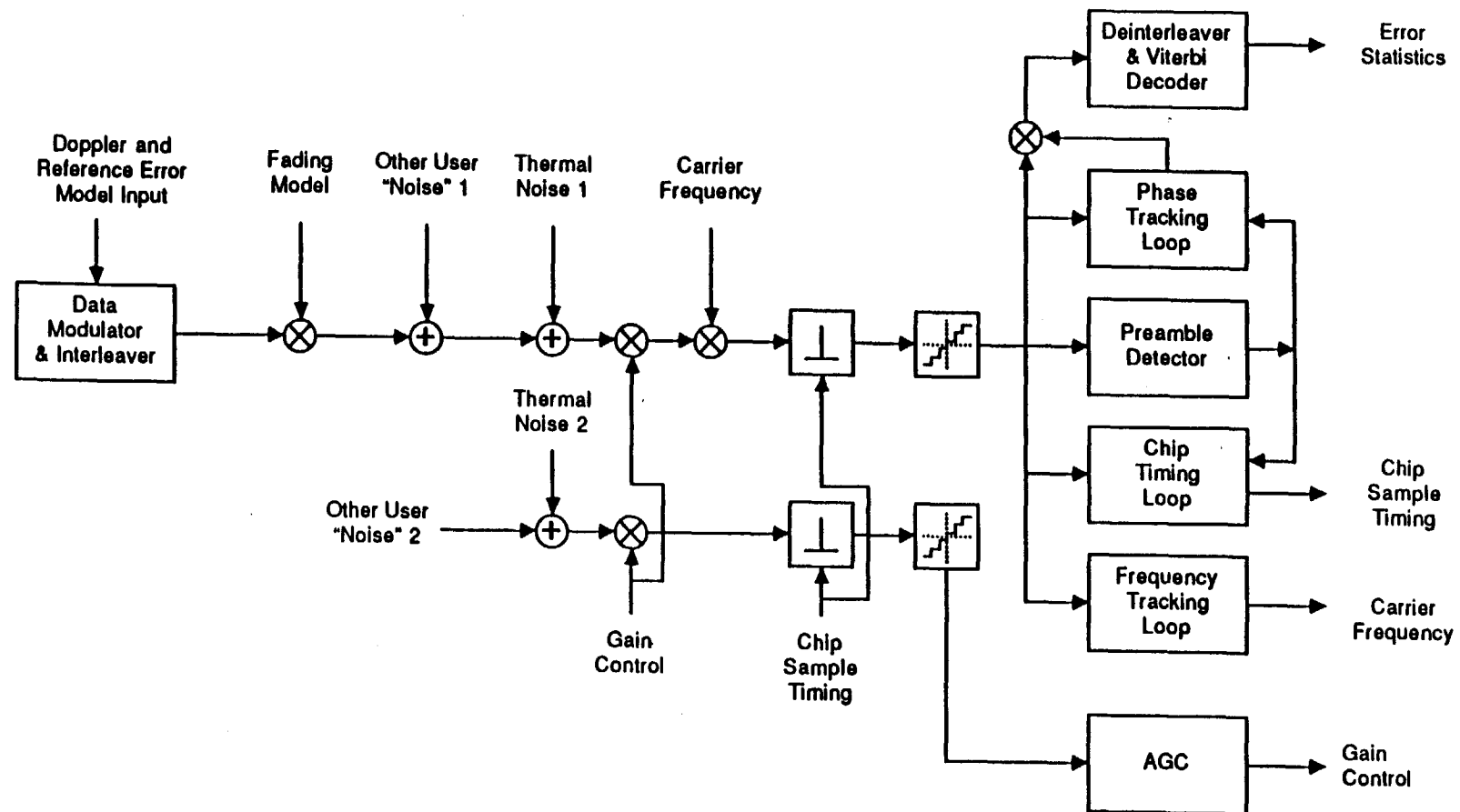
Figure 6-3
Mobile to Hub Processes Modeled by Simulation (BPSK)
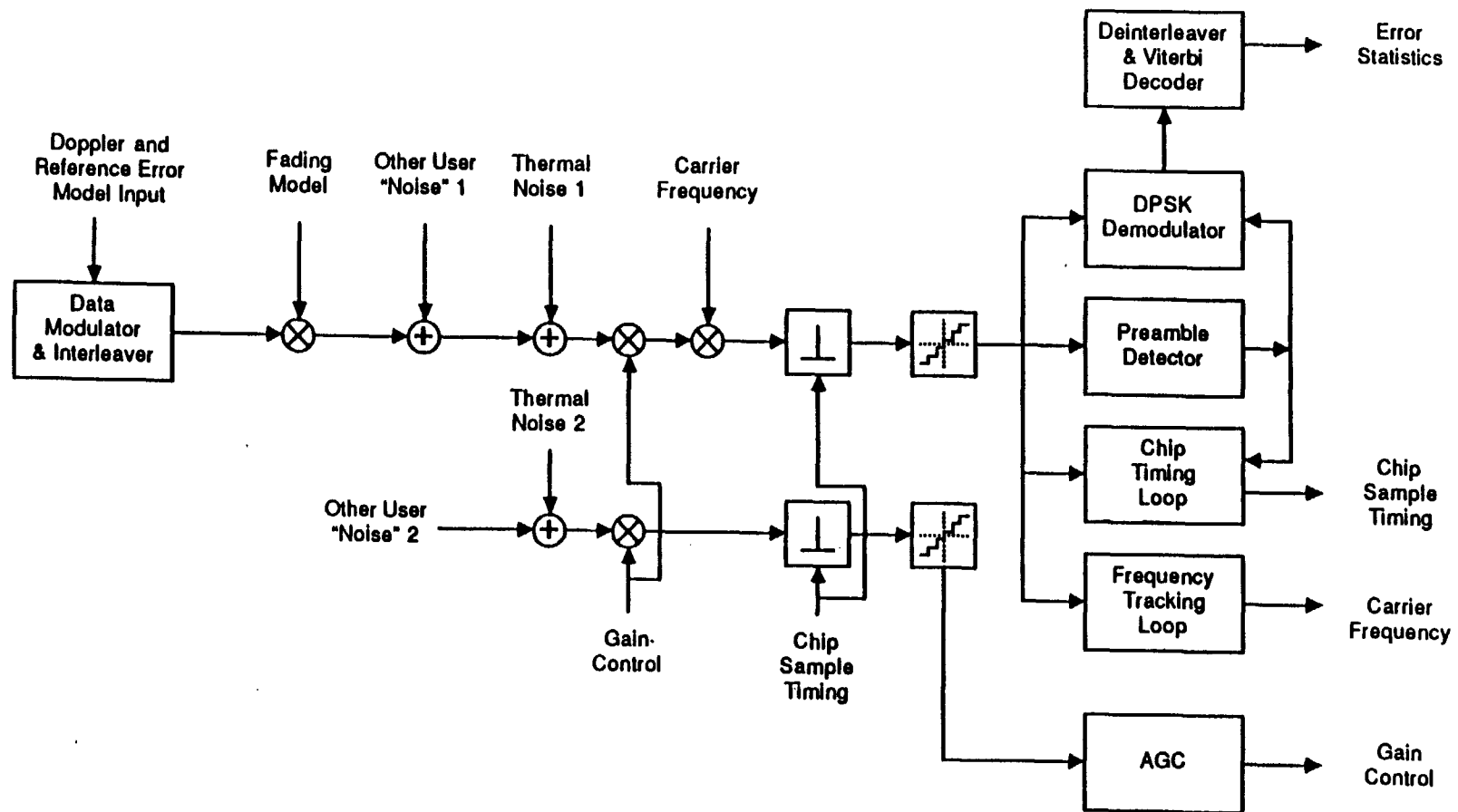
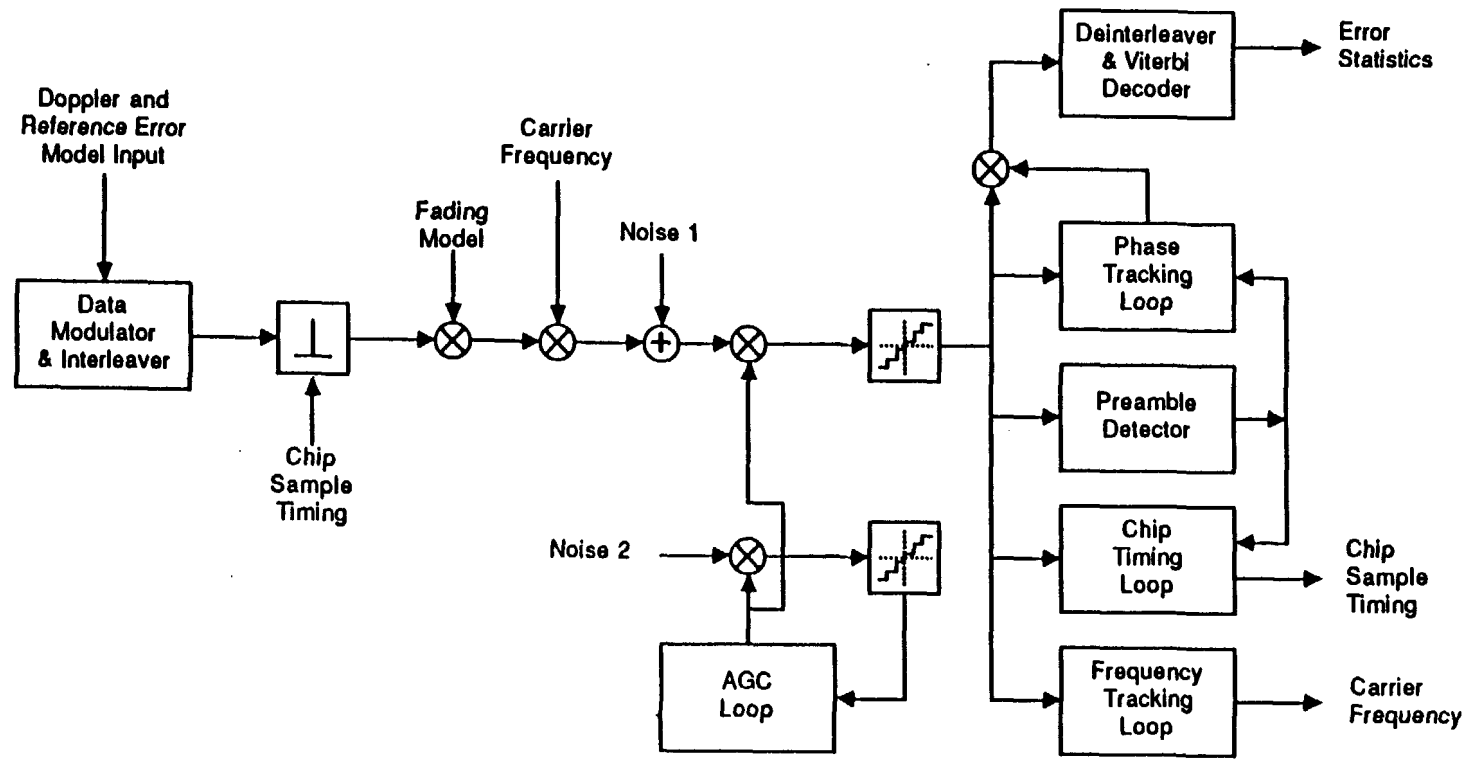**Figure 6-4**

Mobile to Hub Processes Modeled by Simulation (DPSK)

Figure 6-5
Mobile to Hub Simulation Flow (BPSK)
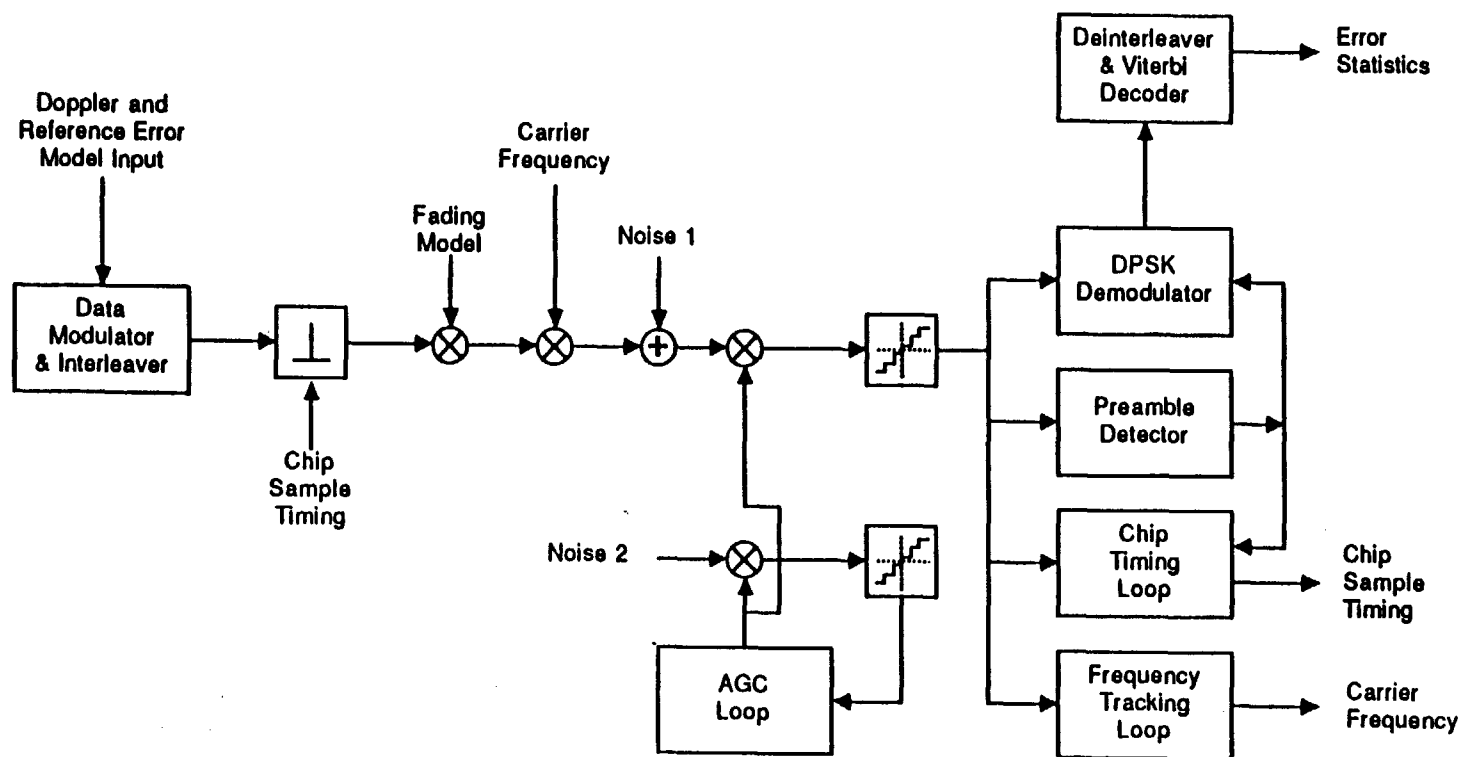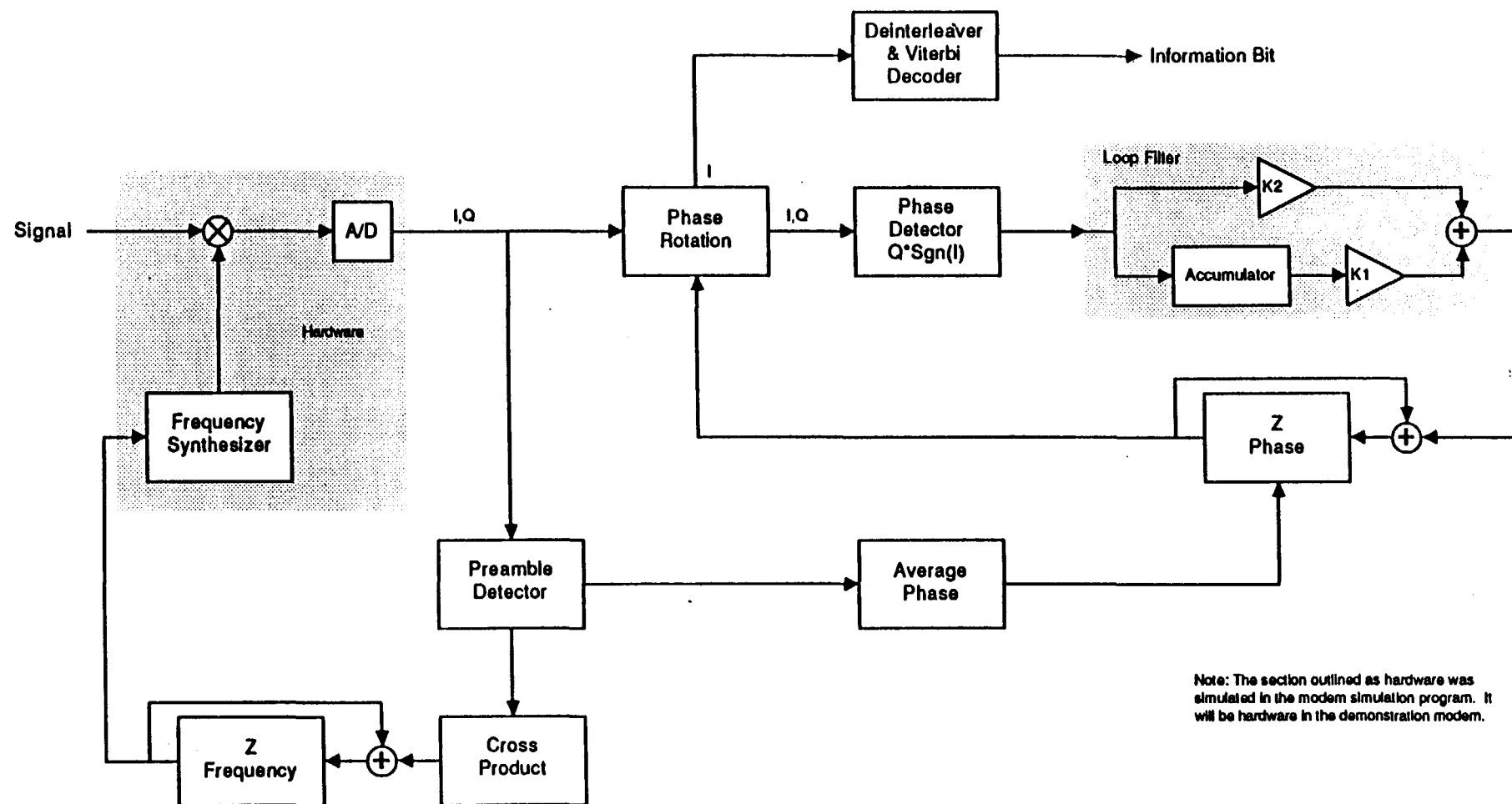
Figure 6-6
Mobile to Hub Simulation Flow (DPSK)

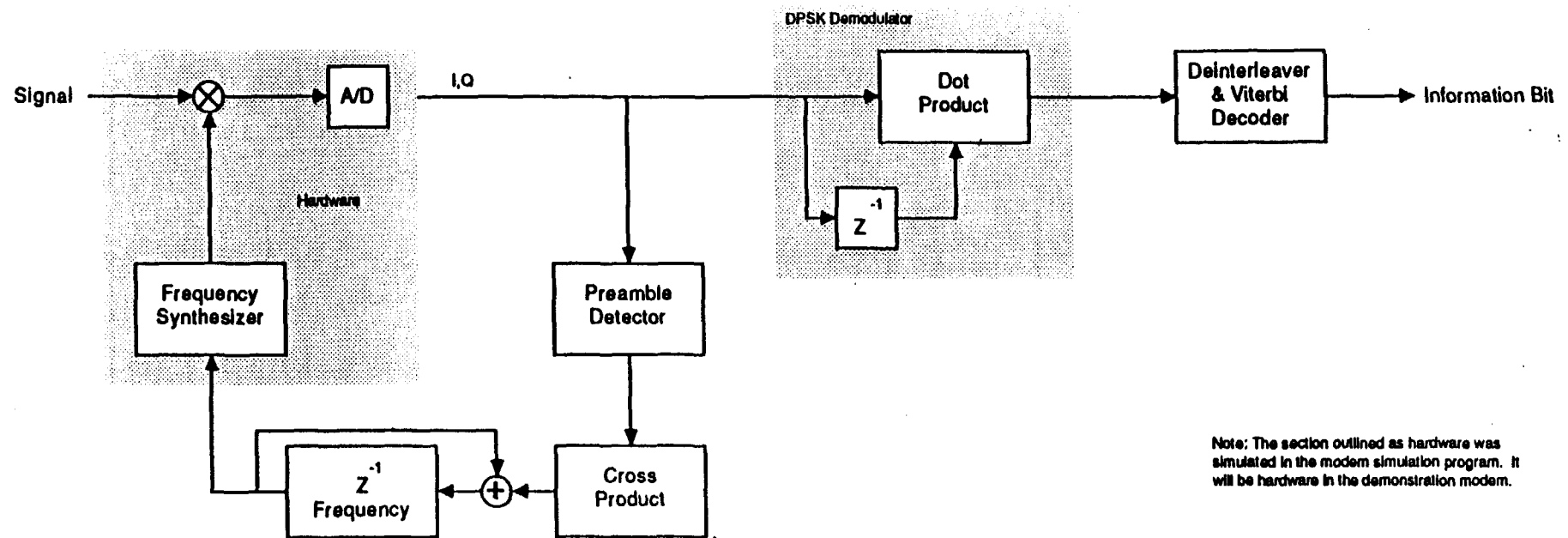**Figure 6-7**
Hub BPSK Frequency and Phase loops

Figure 6-8
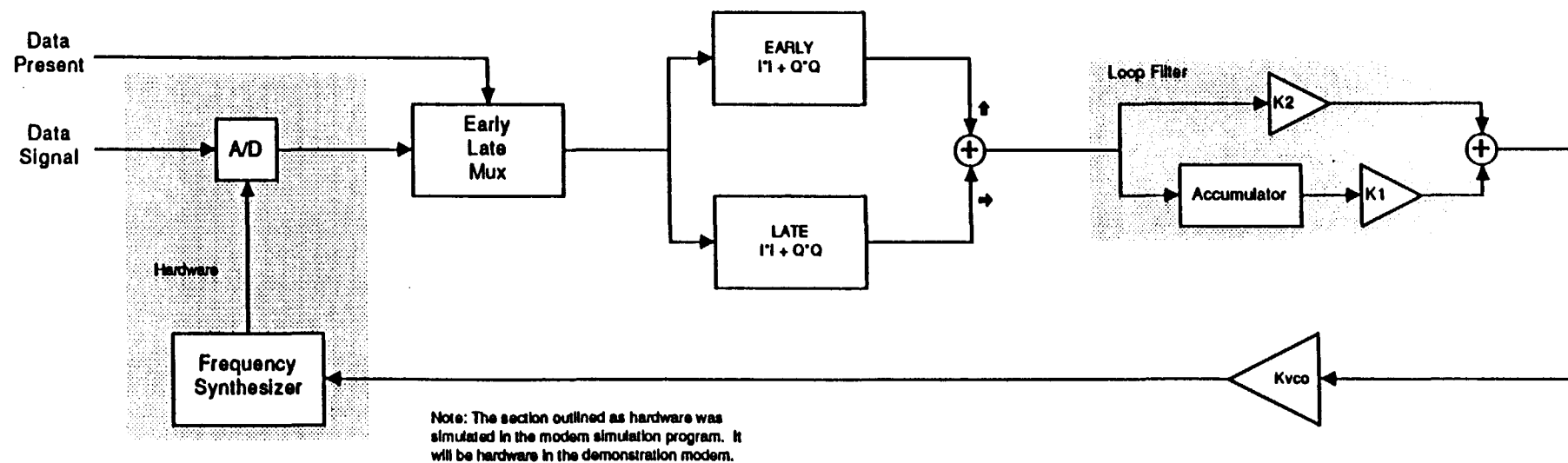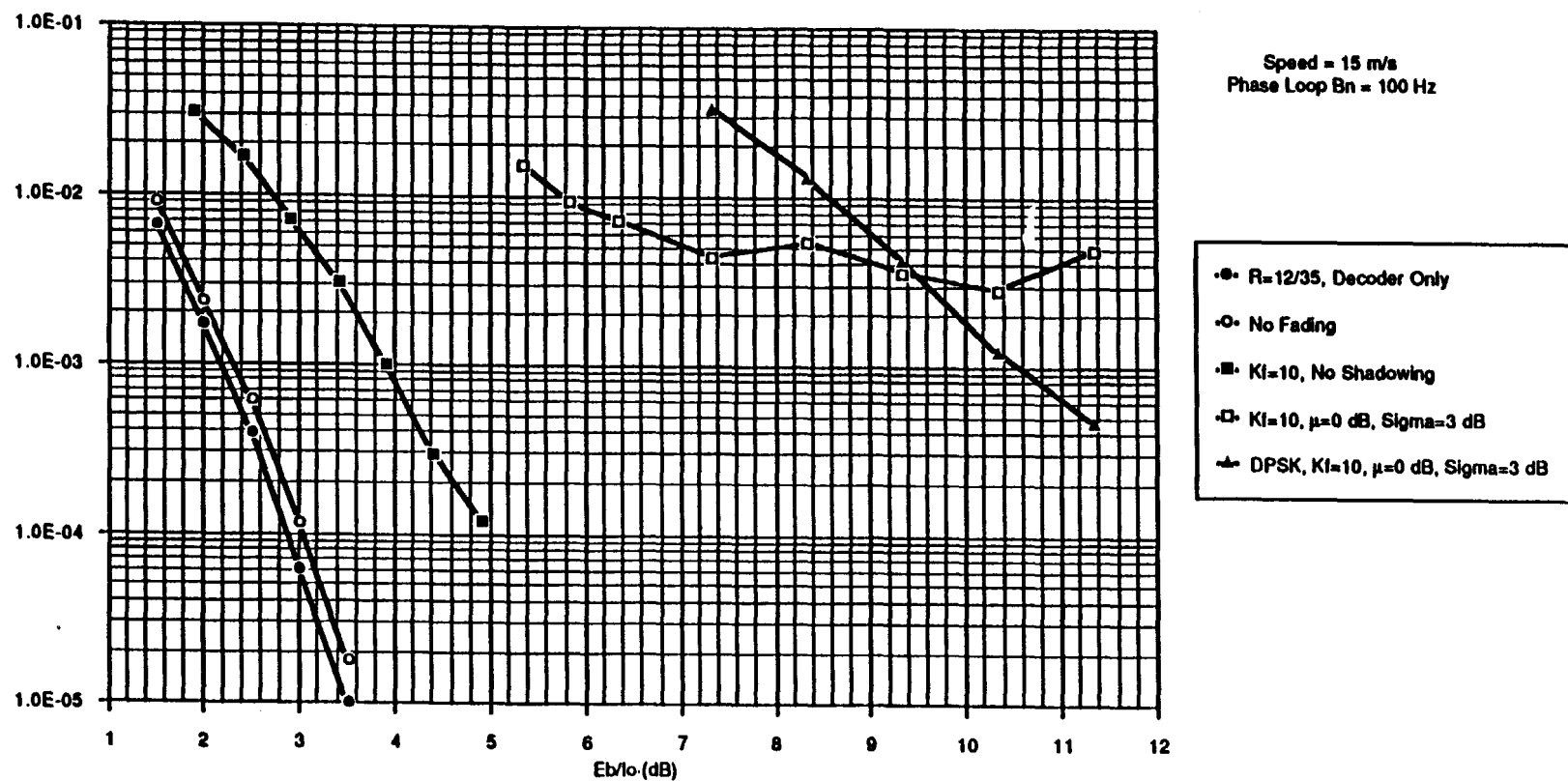**Hub DPSK Frequency loop and Demodulator**

Figure 6-9
HUB Time Tracking Loop

Figure 6-10
Mobile to Hub Bit Error Rate (BPSK)